Rapid Environmental Changes Accompanying Tornadogenesis

Submitted on January 14, 2015 to

Journal of Geophysical Research

Steven E. Koch
NOAA National Severe Storms Laboratory (NSSL)

Randolph Ware
Radiometrics Corporation,
National Center for Atmospheric Research (NCAR), and
Cooperative Institute for Research in the Environmental Sciences (CIRES)

Hongli Jiang
NOAA Earth System Research Laboratory and
Cooperative Institute for Research in the Atmosphere (CIRA)

Marta Nelson
Radiometrics Corporation

Corresponding author: Steven E. Koch, NOAA National Severe Storms Laboratory, 120 David L. Boren Boulevard, Norman, OK 73072 (Steven.Koch@noaa.gov)

Key Points

- Rapid destabilization and increasing shear occurred prior to tornadogenesis
- Local changes revealed by microwave radiometer and wind profiler

Abstract

This study documents the rapid evolution in convective instability and wind shear parameters in the mesoscale environment shortly before the development of a highly unusual tornado that struck Windsor, Colorado. These changes were seen by a ground-based microwave radiometer, a microwave wind profiler, and in a 1-km resolution variational mesoanalysis system, which assimilated data from these observing systems, in addition to conventional data including WSR-88D Doppler radar data. Merged wind profiler-mesoanalysis data revealed that the storm-relative helicity in the lower troposphere jumped to very large values about 90 min prior to tornado touchdown. This change was due to the descent of a mid tropospheric layer of strong vertical wind shear, which was associated with radiometer-detected pronounced decrease in equivalent potential temperature and erosion of the capping inversion. Over the five hours prior to tornadogenesis, the radiometer showed a steady increase of convective instability and reduction of the Convective Inhibition to zero values. The radiometer also revealed a sudden surge in convective instability in the lowest 300 m of the atmosphere in the 90 min prior to development of the tornadic supercell storm, which happened concurrently with explosive increases in storm-relative helicity. The confluence of these local changes at low levels in such a short period of time was likely critical in explaining how this rare tornadic event could have happened so suddenly. This study suggests that two temporal scales were operative – the near-storm environment (90 min) and the storm-scale (30 min).

Index Terms and Keywords

3307 Boundary layer processes
3314 Convective processes
3329 Mesoscale meteorology
3360 Remote sensing

1. Introduction

Forecasting the initiation and evolution of severe local storms is challenged by the need to monitor mesoscale fields of potential instability, moisture availability, vertical wind shear, and vertical circulations at temporal and spatial scales important to nowcasting convection [*Weckwerth and Parsons,* 2004]. Nowcasting is a blend of extrapolation, statistical, heuristic, and numerical prediction techniques for forecasting with local detail over a period from the present to a few hours ahead. Although rapid advances in nowcasting capabilities have been demonstrated with numerical modeling over the past couple of decades, according to *Dabberdt et al.* [2005], "the full benefit of enhanced forecast model resolution has not been and will not be realized without commensurate improvements in high-resolution meteorological observations, as well as improvements in data assimilation, model physics, parameterizations, and user-specific analyses and forecast products." *National Research Council* [2009] argued for the creation of a nationwide mesoscale network comprised of a variety of ground-based sensor systems to address severe limitations in both horizontal and vertical sampling of the atmosphere; specifically, 50–200 km spacing was suggested to capture mesoscale processes important for monitoring and predicting severe thunderstorms. In a follow-on report [*National Research Council* [2010], it was further recommended that profiles of wind, temperature, and moisture should extend to 3 km above ground level (AGL). In a comprehensive assessment of thermodynamic profiling systems for forecasting convection, *Hardesty et al.* [2012] stipulated temperature and moisture profile measurements with at least 1°C and 1 g kg^{-1} accuracy, respectively, a vertical resolution of at least 100 m, and that these measurements should be attended by wind profiling systems for maximum impact. Currently, the spatial coverage of ground-based sensors is much poorer than recommended in these comprehensive reports. The potential positive impacts of assimilating thermodynamic profiler observations from such networks with sufficient density and coverage have been illustrated in numerical data sensitivity experiments [*Ziegler et al.,* 2010*; Otkin et al.,* 2011*; Hartung et al.,* 2011].

For prediction of convection initiation, even stronger requirements are needed: a time resolution of 15 min, vertical resolution of <300m (30m close to the surface), horizontal resolution of <10km, and bias error <5% for moisture and wind in the lower troposphere. The reason for such strict demands on observing systems for severe storm applications can be understood as follows. Moist boundary layer air may be capped by a strong inversion, particularly in "Tornado Alley" in the central U.S., allowing the buildup with diurnal heating of substantial convective available potential energy (CAPE). Once the cap is broken, the ensuing thunderstorms may quickly become severe, as an explosive situation is created where the triggering of storms and accurate knowledge of the moisture distribution become critical. In this region, there can exist very large horizontal gradients (>1 g/kg/km) in water vapor mixing ratio across the "dryline", a well-known phenomenon associated with explosive development of severe local storms. A strong association between the dryline location and convection initiation (CI) is easily understood because the dryline is also located within a horizontal gradient of virtual potential temperature and flow deformation, which promotes a solenoidal vertical circulation via frontogenesis [*McCarthy and Koch*, 1982; *Ziegler et al.,* 1995; *Buban et al*., 2007]. Mesoscale fluctuations in the moisture gradients *along* the dryline also can be very important in CI [*Koch and McCarthy*, 1982; *Atkins et al.,* 1998]. Storms may also form at a "triple point" where a baroclinic boundary and the dryline intersect [*Weiss and Bluestein* 2002; *Wakimoto et al.* 2006]. The magnitude and depth of lifting (i.e., vertical circulations) at boundaries such as the dryline, fronts, and outflow boundaries are important factors in thunderstorm development and character, as is the manner in which the ambient wind shear profile interacts with the thermodynamic fields near the boundaries (*Wilson et al.,* 1998]. Also, areas of small-scale vertical vorticity referred to as "misocyclones" found along drylines and other boundaries are suspected to play a role in CI [*Buban et al.,* 2012].

Rasmussen and Blanchard [1998] found that vertical wind shear and CAPE parameters assessed from proximity soundings discriminated strongly between nonsupercell thunderstorms, supercells without significant tornadoes, and supercells with significant tornadoes. *Thompson et al.* [2003] determined that vertical wind shear and moisture within 1 km of the ground could discriminate between nontornadic and significant tornadic supercell storms. *Feltz and Mecicalski* [2002] used 10-min sampled Atmospheric Emitted Radiance Interferometer (AERI) data to illustrate how large changes in the strength of the capping inversion, boundary layer moisture, and trends in bulk atmospheric stability can occur in the few hours prior to the rapid development of severe convection. In another study using AERI data, *Wagner et al.* [2008] found that CAPE *gradually* increases in the 6 h prior to CI, reaching a peak roughly 1 h before a tornado or large hail forms, whereas for nontornadic storms, CAPE reaches a maximum nearly 3h before CI. Coincident wind profiler data showed that wind shear and storm-relative helicity [SRH] for both tornadic and nontornadic storms started to increase roughly 3h before an event. The value of SRH [*Droegemeier et al*., 1993] has been shown in numerous studies to be one of the most useful parameters governing the likelihood of supercell storms capable of producing large hail, damaging winds, and tornadoes. Environments with large levels of SRH support longer-lived storms than those that form in atmospheres with lesser levels of SRH.

The above-cited studies have illustrated the value of special ground-based observations to monitor the mesoscale severe storm environment. Observing systems that are capable of sampling the boundary layer with at least moderate vertical detail include radars; commercial aircraft on ascent and descent; rawinsondes; and ground-based infrared and microwave radiometric soundings, wind profilers, sodars, and lidars. Among these observing systems, microwave radiometric profilers (MWRP) and wind profilers appear to have the greatest potential for *continuous* monitoring even in the presence of precipitation throughout the *entire* depth of the boundary layer with at least moderate vertical resolution. *Ware et al.* [2014] and *Xu et al*. [2014] showed that MWRP are able to provide useful, though somewhat degraded, information even in the presence of heavy precipitation (>25 mm/h) by use of neural network methods to retrieve temperature, humidity and liquid profiles from off-zenith (15° elevation) observations. Generally, the vertical resolution of both microwave and infrared passive remote sensors is best close to the surface and degrades rapidly with height (though less rapidly for infrared). Lidars provide higher resolution and greater accuracy than passive remote sensing systems, but are limited to the clear air or optically thin clouds.

MWRP and radar wind profilers have been utilized before in studies of the local storm environment and mesoscale triggering phenomena such as cold fronts, drylines, gust fronts, bores and gravity waves [*Koch and Clark,* 1999; *Benjamin, et al.,* 2004; *Knupp et al.,* 2009; *Madhulatha, et al*. 2013]. Large changes in thermodynamics and integrated water vapor have been observed to occur within a few hours prior to thunderstorm formation from such systems [*Güldner and Spänkuch*, 2001], and occasionally just 30 min when associated directly with the trigger mechanism's vertical circulation [*Koch and Clark*, 1999]. The present study demonstrates the tremendous value offered by the use of MWRP and wind profilers in capturing very rapid and important changes in the local environment of a strong tornado that developed near the intersection of a dryline and warm front.

2. Data and Methodology

This study is of an unusual tornadic event that occurred near Windsor, Colorado (about 80 km north of Denver) on 22 May 2008. Special observations available for this study included a ground-based microwave radiometer and radar wind profiler that detected temporal changes in convective parameters with 5-6 min sampling. Also, a very high-resolution mesoanalysis and prediction system was used to relate the rapid changes detected by the profilers to the mesoscale environment of the tornado. The radiometer was located 53 km southwest of Windsor in Boulder, whereas the wind profiler was about 30 km south of Windsor at Platteville. The tornado touched down within 2 km of the Platteville Wind Profiler, damaging the profiler and other instrumentation at the site and causing some loss of data as discussed below. The mesoanalysis domain and the positions of Windsor, the Boulder radiometer, the Platteville wind profiler, and the local NWS-Denver rawinsonde are shown in Fig. 1.

2.1. Microwave radiometer

Microwave radiometers can obtain vertical profiles of temperature and water vapor density under all weather conditions at time intervals of a few minutes or even faster [*Hardesty et al.*, 2012]. Two radiometers were used in this study: a 12-channel Radiometrics MP-3000 and an uncalibrated 35-channel version of this instrument (MP-3000A) [*Ware et al.,* 2003; *Güldner and Spänkuch*, 2001; *Cimini et al*., 2006, 2011]. The MP-3000 observes brightness temperatures related to atmospheric moisture in 5 frequency bands from 22–30 GHz and atmospheric temperature in 7 bands from 51 to 59 GHz. Cloud base height is automatically determined by mapping zenith infrared temperature observations from a 9.6-11.5 μ radiometer to the retrieved temperature profile. The radiometer has automated elevation and (an optional) azimuth scanning capability. In situ surface temperature, humidity, and pressure sensors provide surface conditions used in the retrievals. Although the sampling rate of this radiometer can be as short as 10 s, we used filtered 5-min data for this study for maximum accuracy. Typical RMS errors associated with temperature and humidity retrievals from this radiometer [*Güldner and Spänkuch*, 2001; *Liljegren, et al., 2004; Cimini et al*., 2011] are 0.6 K near the surface, increasing to 1.6 K at 7 km, and 0.25 g m^{-3} error near the surface, increasing to 0.90 g m^{-3} at 2 km, respectively (these are smaller than radiosonde representativeness errors). The effective vertical resolution of the MWRP degrades with height, being best near the surface (~50 m) and decreasing to ~ 250 m at 2 km, allowing mixing layer height measurements [*Cimini et al, 2013*], but making the detection of mid-tropospheric inversions difficult. The off-zenith correction technique mentioned earlier was applied in the current study.

The "inverse problem" in radiative transfer (determination of profiles of temperature and water vapor from multi-channel radiances) is ill posed, meaning that its solution is neither unique nor stable. Accordingly, *a priori* knowledge of the atmospheric variable (temperature and water vapor) is needed to constrain the solution to obtain those variables from the measured brightness temperatures. A popular method, used herein, is to employ a neural network retrieval technique trained with several years of historical radiosonde soundings from a location with similar altitude and climatology to the radiometer site (*Ware et al*., 2003; *Cimini et al.* 2006; *Knupp et al.* 2009; *Madhulatha et al.* 2013). Alternatively, one-dimensional Variational Retrieval (1DVAR) can optimally couple MWRP observations with numerical weather prediction (NWP) model analyses or forecasts to obtain temperature, humidity and liquid water content retrievals [*Hewison, 2006; Cimini et al., 2011*]. The 1DVAR retrievals retain the information from the NWP system in the upper troposphere (where it is typically more representative of the actual atmospheric state than from the radiometer), while being able to correct inaccurate model analyses in the lower troposphere (within 2 km of the surface) where the MWRP has the greatest value.

Accurate surface temperature data (with representativeness error < ±1.8 C) are needed for optimum radiometer retrieval accuracy. Regrettably, since the Radiometrics systems were engaged in manufacturing and engineering testing on 22 May 2008, they were operating with less than optimal accuracy. Specifically, the fan that aspirated the surface temperature and relative humidity sensors on the 12-channel MP-3000 was not operating to specification; consequently, early results of performing radiative retrievals using the bad infrared sensor showed significant warm biases and unrealistically large superadiabatic lapse rates. Hence, we substituted the aspirated surface data from the infrared sensor attached to the MP-3000A for that on the well-calibrated MP-3000 even though the former microwave sensors were not validated by recent calibration. Further discussion of this matter and cross-validation results appear in section 3.

2.2. Radar Wind Profiler

Another ground-based observing system used in this study was a NOAA Wind Profiler [*Chadwick and Hassel,* 1987] operating at a frequency of 404.37 MHz. The Profiler has a fixed phased-array, coaxial–collinear grid antenna with three beams (at zenith and 16.3° off-zenith). By observing refractivity gradients in the clear air, these wind profilers are able to generate a profile of winds every 6 min except in the presence of heavy precipitation, when the assumption of horizontal homogeneity of the wind field across the three beams may be violated. The radar profiler samples in two modes with differing vertical resolutions; however, since no observations higher than 6 km in altitude are used in this study, all observations here have a 250-m vertical resolution.

Radar wind profilers exhibit excellent agreement with rawinsonde observations, and have been shown to be of tremendous value in forecasting the likelihood of supercell storm occurrence and attendant severe weather [*Benjamin et al.,* 2004]. Vertical wind shear and helicity were calculated at 6-min intervals from the Wind Profiler in combination with the 15-min analyses produced by a variational version of the Local Analysis and Prediction System (vLAPS) following application of a method (described below) to fill several Profiler data gaps, and to replace nonexistent Profiler data after 1600 UTC by the vLAPS analyses.

2.3. Variational mesoanalysis and prediction system

A 1-km version of vLAPS coupled with the Weather Research and Forecasting (WRF) model was used in this study to relate the excellent temporal details provided by the ground-based profiling observations to the mesoscale environment of the tornado. The first guess fields for a 3-km version of vLAPS came from the 12-km resolution NAM212. The vLAPS analyses acted as initialization fields for the WRF/ARW to generate 3 km forecasts. The model was initialized at 1200 UTC and forecasts were produced out to 0000 UTC 23 May 2008. These 3-km WRF model forecasts were then used as the first guess (background) to create the 1-km vLAPS analyses from bilinear interpolation beginning at 1230 UTC. It is these fields that are shown in this paper.

The vLAPS assimilated data from the wind profiler and radiometer; reflectivity and radial wind data from National Weather Service WSR-88D radars; soundings, cloud-track winds and total precipitable water from geostationary satellite; aircraft data; ground GPS-Met sensors; and other conventional data. Only the lowest 1 (2) km of temperature (water vapor) data retrieved from the radiometer were used by vLAPS, but the entire 16 km of wind profiler data was assimilated into vLAPS.

Basically, vLAPS is a variational extension of the original LAPS [*Albers et al.,* 1996; *Hiemstra et al.,* 2006], which for years used a simple two-pass, distance-weighting objective analysis scheme [*Koch, et al.,* 1983] with dynamic balancing. LAPS pioneered an approach called "hot start", whereby variables strongly affected by deep, moist convection such as vertical velocity, temperature, moisture, and cloud microphysical properties are analyzed and mutually adjusted to fully capture moist diabatic processes. In the variational version of LAPS developed recently [*Xie et al.,* 2011], a multigrid technique is adapted to efficiently solve the variational minimization problem, and a Laplacian filter is used to approximate the scale-dependent background error covariance and apply dynamic constraints applicable at different multigrid scales. The hot start cloud analysis has been favorably tested at spatial resolution down to 1 km, which is the grid size used in the present application.

Table 1 summarizes the data availability for this study. The microwave radiometer produced data over the entire 24-h period. The wind profiler produced nearly continuous data until 1600 UTC, when it was shut down as a precaution because of the expectation of severe weather. The vLAPS system was initialized at 1300 UTC and was used in conjunction with the other data through 0000 UTC 23 August 2008.

3. Case Overview and Analysis Verification

The event to be discussed herein was a strong EF3 tornado that occurred at Windsor, Colorado just before noon on 22 May 2008. This event was unusual for a number of reasons. First, the Front Range of the Rocky Mountains is unaccustomed to strong tornadoes, particularly ones that occur in the morning. The tornado then took a very uncommon track to the northwest, displaying the longest track of any recorded tornado with a westward component in this region, and in fact, the only EF3 tornado ever recorded near the Front Range with such a track.

Schumacher et al. [2010], hereafter S10, provide a good overview of this case, including synoptic- and mesoscale factors that may have played important roles in the development of the tornadic storms. Briefly summarizing their findings, this event included a southerly upper level jet streak exceeding 40 m s^{-1}, a pronounced low pressure center located just east of Denver, a strengthening warm front to the east-northeast of the low and a dryline to its south. Dry, gusty, southerly winds developed to the west of the dryline, while southeasterly winds advected warm, moist air to the east of the dryline, and cool, northeasterly flow conditions existed north of the warm front. S10 estimated CAPE values > 2000 J kg^{-1} and storm-relative helicity of 219 m^2 s^{-2} in the 0–1 km layer using a Denver 1800 UTC sounding (released ~100 km to the south of the warm front) that was modified to account for the surface conditions in the local vicinity of Windsor. These CAPE and helicity values are consistent with supercell thunderstorm environs [*Thompson et al.* 2003]. As will be shown, local destabilization and increasing vertical wind shear occurred much more rapidly than estimated in the S10 study, reaching considerably higher values than they reported.

S10 reported a lifting condensation level of ~1.0 km AGL, which is an unusually low altitude for eastern Colorado. This value was determined for a cloud-covered region just north of the warm front. The stratus clouds immediately to the south of the front rapidly dissipated by 1600 UTC, allowing substantial solar radiation to warm the surface. In summary, the air entering the Windsor storm at cloud base was exceedingly moist, unstable, and containing plentiful vertical wind shear. The mesoscale lifting mechanism needed to "trigger" the formation of deep convection was indeterminate.

The first severe thunderstorm warning was issued at 1109 LT (1709 UTC), the tornado warning was issued just 9 minutes later, and the first tornado touchdown was reported at 1126 LT 25 km southeast of Windsor (within 2 km of the location of the wind profiler used in this study). Both warnings were issued before the Storm Prediction Center had issued a tornado watch (at 1125 LT). S10 surmised that the early initiation of the storms and their very rapid development in such an unusual setting as this may have played a role in the tornado watch not being issued until after the first warning was issued.

The Windsor storm is shown from radar and satellite perspectives in Fig. 2. The warm front is barely discernible in Fig. 2c as a short curved arc of low reflectivity stretching east of the storm. Note the northwesterly motion of the storm. The unusual location and orientation of the "hook echo" in Fig. 2a, which was located on the southeastern side of the storm and turned 90^o counterclockwise from a normal alignment, and the existence of a crisp anvil edge to the cumulonimbus cloud on this same side, reveal that the deep tropospheric wind shear was from the south-southeast. The Windsor tornadic storm actually reinvigorated after crossing over the warm front and headed northwestward to Laramie, Wyoming, where it spawned a second tornado that has been examined by *Geerts et al.* [2009].

Before discussing the results of our analyses, the accuracy of the radiometer and wind profiler observations should be established. Profiles of thermodynamic retrievals (using the surface IR data from the MP-3000A) from the calibrated 12-channel radiometer are compared to the NWS-Denver rawinsondes at 1800 UTC 22 May and 0000 UTC 23 May in Figs. 3a and 3b, respectively. The temperature profiles from the MWRP are in excellent agreement with those measured by the two rawinsondes throughout the entire atmosphere below the tropopause (350 hPa), though as discussed earlier, the weak mid-tropospheric inversions are not detected by the radiometer. The water vapor profiles at 0000 UTC are in overall good agreement, but there are systematic differences in moisture profiles between the radiosonde and radiometer at 1800 UTC. We believe those differences are real, a reflection of the significant difference in moisture across the warm front, with the radiometer being located within the deep clouds to its north, whereas the drier Denver radiosonde was taken within partly sunny conditions south of the front. This disparity is not present 6h later, by which time the dryline had passed through the area. The cloud base levels measured by the radiometer at 1800 UTC (not shown) indicated that clouds descended to the surface in the pre-dawn hours and that low clouds and fog continued through 1600 UTC. This is consistent with the available surface reports and satellite imagery.

A sample radiometer-derived sounding for 1706 UTC (Fig. 4) – selected because it was the time at which the radiometer exhibited the highest value of Surface-Based CAPE (SBCAPE) – shows a substantial amount of "positive area" for a parcel lifted from the surface. The computed Lifting Condensation Level (LCL) of 605 m AGL matches the Level of Free Convection (LFC), i.e., no Convective Inhibition (CIN) existed at all at this time. The inset in this figure shows that the combination of 0–4 km wind shear (from the Denver sounding) of 30 m s^{-1} and SBCAPE of 2866 J kg^{-1} (from the radiometer) places this sounding solidly into the supercell category. Furthermore, strong veering of the winds from an easterly direction in the lowest 1 km above the surface to very strong south-southeasterly at 5 km MSL (3.5 km GL) results in a Storm-Relative Helicity (SRH) value of 134 m^2 s^{-2} in the 0–1 km layer, though as is shown below, even this special rawinsonde greatly underestimated the SRH present in the near-storm environment near Windsor. These thermodynamic and shear parameters are all consistent with the single-sounding estimates provided by S10 as mentioned earlier, though notably stronger given the greatly improved temporal sampling by the radiometer, and its closer proximity to the genesis of the storm cloud that spawned the tornado.

Time series of 0–1 km storm-relative helicity (SRH) from the Wind Profiler and the vLAPS analysis over the period 1310–1550 UTC are compared in Fig. 5. Despite a minor offset of ≤ 50 m^2 s^{-2}, the two traces show a similar slow upward trend in helicity values with time, as depicted by the lines of regression. We judge this comparison (as well as a direct comparison of the wind profiles (not shown)) to provide sufficient justification for merging the two datasets by inserting the vLAPS winds interpolated to the Platteville Profiler site after 1600 UTC.

4. Results and Discussion

4.1. Radiometer-derived thermodynamics

The radiometer provided excellent temporal and vertical continuity in retrieved water vapor mixing ratio and equivalent potential temperature over the altitude range from the surface to 5 km AGL (Fig. 6a, b). A number of features of considerable meteorological interest can be seen. First is the sudden increase in the depth and magnitude of water vapor at 0530 UTC reflecting the passage of the pronounced warm front over the region the night before the tornado outbreak. The radiometer revealed that the depth of the surface-based layer of rich moisture >8 g/kg increased for the next several hours, but then remained relatively constant until just before the tornado occurred at ~1726 UTC at the Platteville wind profiler site (47 km northeast of the radiometer). Dryline passage occurred at 1815 UTC, causing a sudden drastic reduction of moisture content.

Of particular interest is the pronounced surge in low-level moisture appearing from 1730–1800 UTC during nearby passage of the tornado. The sudden increase in very low-level moisture during tornadogenesis also occurred in association with rapid destabilization, as may be inferred from the rapid decrease of equivalent potential temperature θ_e with height in the lowest 1 km layer at 1730 UTC (Fig. 6b). A better understanding of this lower tropospheric process is provided by Fig. 7, which displays the temporal variation of θ_e (Fig. 7a) and potential instability (decrease of θ_e with height, or a negative θ_e gradient) derived from the radiometer in the 1000m layer immediately above the ground. This analysis reveals that the extremely rapid destabilization (Fig. 7b) actually occurred in a very thin layer near the ground, beginning at 1630 UTC and ending at 1730 UTC, with a strong maximum near the time of nearby tornado passage. The cause of this destabilization was that, as the clouds began breaking up in the Windsor-Platteville-Boulder triangle region precisely at this time, solar heating could warm the surface layer.

Closer inspection reveals that a slightly elevated layer of strong, localized instability began two hours earlier (at 1430 UTC), and that this layer ~ 200m above ground occurred because of decreasing θ_e centered at the 350 m level (Fig. 7a). In fact, a comparison of this detailed display of θ_e in the lowest 1 km with that in Fig. 6b for the lowest 5 km of the atmosphere reveals that this layer of decreasing θ_e appearing in the hour between 1600 and 1700 UTC was the lowermost extension of a much deeper layer of decreasing θ_e extending to at least 600 hPa. The cause of this feature is still under investigation using the vLAPS analysis, and will be reported on in a future paper. One possibility being examined is that this low θ_e air had its source in adiabatic cooling as air was advected from the southeast and lifted over the Palmer Lake Divide, a plateau-like region of higher terrain just south of Denver, which has been noted in other studies to be important for convection initiation in the Denver region [*Szoke et al.* 1988].

The combination of surface-based and lower-tropospheric destabilization processes resulted in extremely rapid increase of CAPE in a short period of <60 min before the tornado appeared. CAPE calculated from the radiometer reached a peak at 1706 UTC of 2866 J kg^{-1}, just 20 min before the tornado made its appearance (Fig. 8a). It is apparent that this value was attained quite suddenly between then and 1615 UTC, when a relative minimum occurred following several hours of gradual increases. Finally, an abrupt decrease of CAPE denotes the passage of the dryline at 1800 UTC. During the several hours when θ_e was increasing, CIN was gradually declining, and actually reached zero values just minutes before the onset of rapid CAPE increases that began at 1615 UTC (Fig. 8b). The combination of no perceptible inhibition to air parcels reaching their Level of Free Convection (cf. Fig. 4) and suddenly abundant CAPE resulted in explosive convective initiation beginning at 1630±15 min, and the very rapid evolution of the Windsor storm into a tornadic supercell. Of course, sufficient vertical wind shear is a necessary ingredient for that to happen, to which we turn next.

4.2. Profiler and vLAPS-derived winds and vertical shear

A time-height display of raw data obtained from the Platteville wind profiler is displayed in Fig. 9. Only data in the lowest 8 km AGL is shown, since the focus of this study is on processes in the low-to-mid troposphere, though profiler data did extend to 16 km. This plot shows 6-min horizontal wind vectors from 1300 through 1600 UTC, which unfortunately is the last time data was produced prior to the instrument being shut down in preparation for expected severe weather. Calculation of the horizontal winds from the radial velocities along each beam was accomplished trigonometrically, assuming horizontal homogeneity of the wind field across all beams [*Chadwick and Hassel,* 1987]. While this assumption is nearly always reasonable for long averaging periods on the order of an hour, it may be violated for averaging periods on the scale of minutes when variations in instantaneous wind exist from beam to beam. The assumption of homogeneity is typically violated, and accurate wind measurements are impossible to obtain, in the presence of convective precipitation. There are several data dropouts in Fig. 9 due to low signal-to-noise, primarily at some of the upper data gates because this assumption was violated. In order to provide a continuous, uniform display of the data, the quality control and analysis techniques developed by *Trexler and Koch* [2000] were adapted to this data. Their technique includes a two-pass Barnes objective analysis application to the wind components to interpolate the data to a regularly spaced grid in order to fill small gaps in the data. The resulting wind analysis was then directly merged with the vLAPS analyzed winds interpolated in time and space to the Platteville profiler location after 1600 UTC.

The resulting analysis is displayed in Fig. 10a. The continuity in the wind analysis across the "profiler-vLAPS" interface at 1600 UTC is excellent, lending support to this analysis approach. Several important conclusions can be drawn from this analysis. In the broadest sense, vertical wind shear increases over time, primarily in speed, though the winds at most levels back with time up to when the tornado happened as the upper-level trough was approaching. At low levels, the presence of easterlies after 1000 UTC is associated with the southward sagging of the warm front. The fact that this wind shift occurred 5h later than the first abrupt increase in low-level moisture seen in the radiometer moisture time-height cross section suggests that formation of the warm front occurred in stages; in fact, another look at Fig. 6 reveals a second moisture surge at 0900 UTC that corresponds better with the wind shift. Pronounced increase in wind speeds in the lower troposphere below 3 km occurs after 1600 UTC (note the descent of the 50-kt isotach) in association with the previously discussed thermodynamic changes. A dramatic increase in the low-level easterlies appears in the lowest 1–2 km after 1730. However, the evidence suggests that most of the latter changes were related directly to the passage of the tornadic supercell storm and the subsequent dryline momentum surge, not to near-storm environmental changes. This conclusion is based on the zoomed-in display of the winds in the lowest 3 km over a 2-h period (Fig. 10b) showing that the increasing winds actually occurred immediately after 1800 UTC, or 30 min following the tornado appearance at the profiler. Since the analyses after 1600 UTC are produced by the vLAPS and are not based on wind profiler data, we interpret this disparity to reflect a small temporal error in the analysis/forecast system.

The results of these two pronounced events – the increasing vertical wind shear in the mid-troposphere after 1600 UTC and the dramatic, small-scale increase in low-level shear appearing at 1730–1800 UTC, are that the SRH for 0–1 km, 0–3 km, and 0–6 km layers all displayed sudden jumps at these two times (Fig. 11). Another measure of the validity of the computations from the vLAPS-Profiler merged dataset is that the 0–1 km SRH value of 219 $m^2 s^{-2}$ estimated by S10 using a modified 1800 UTC Denver sounding (the black cross in Fig. 11) is in excellent agreement with that from our analysis at that time. These conclusions are further supported with a time-height plot of vertical wind shear from the merged dataset (Fig. 12): the rapid increase in shear in the 2.0–2.5 km layer after 1600 UTC, and the sudden appearance of impressive low-level shear after 1800 UTC associated with the strong winds from an easterly direction at and immediately following the tornado. We conjecture that the loss of Profiler data after 1600 UTC likely means that the extreme shear present as the tornado passed over the Profiler was under sampled, even in the vLAPS analysis.

We conclude from these analyses that two primary time scales were involved in the Windsor event. First, about 90 min before tornadogenesis, deep tropospheric shear increases occurred in conjunction with the aforementioned mid-to-lower tropospheric decreases in equivalent potential temperature and gradual erosion of the capping inversion and CIN. Then, within ±30 min of the tornado, a second surge of SRH occurred in association with the rapid increases in CAPE. We refer to these scales as the “near-storm environment” and “storm-induced” fields, respectively. To our knowledge, this is the first study that has been able to clearly elucidate these important distinctions with ground-based remote sensing observations and detailed mesoanalysis.

5. Conclusions

The combined availability of a microwave radiometer and a wind profiler in the immediate vicinity of a very powerful tornado, in conjunction with a 1-km resolution variational mesoanalysis/prediction system (vLAPS), provided unprecedented observations of the near-storm environment and storm feedbacks. The loss of wind profiler data ~ 90 min prior to the tornado required its replacement with vLAPS fields, but this data merger did not produce any noticeable discontinuity in the wind profiles. The vLAPS did utilize WSR-88D Doppler radial winds, subjected to dynamical balancing constraints, so the later evolution of the near-storm environment was mostly attributable to the influence of those data. Inaccurate experimental radiometer surface temperature and humidity sensors did not affect the interpretation of the results focusing on meteorologically important temporal changes, as alternative surface temperature and humidity data were available for the retrievals.

The radiometer provided excellent temporal and vertical continuity in retrieved water vapor mixing ratio and potential instability up to 6 km AGL and revealed that a pronounced surge in rich low-level moisture occurred just before and during passage of the tornado. While the radiometer showed a continuous increase of CAPE throughout the morning leading to the development of the tornadic supercell storm, more interestingly, in the hour before tornadogenesis, it revealed a sudden surge in potential instability in the lowest 300 m of the atmosphere as the cloud cover broke and low-level heating and moistening occurred in conjunction with decreases in derived equivalent potential temperatures over a much deeper layer. CAPE calculated from the radiometer reached a peak of 2866 J kg^{-1} just 20 min before the tornado passed nearby.

The combined wind profiler-vLAPS analysis revealed that wind shear rapidly increased just prior to tornado formation in a two-stage process: first, about 90 min prior to tornadogenesis, large increases in mid-lower tropospheric wind shear occurred, which was associated with a downward penetration of low equivalent potential air detected by the radiometer. Storm-relative helicity in the lowest 1 km of the atmosphere jumped from 50 to 350 $m^2 s^{-2}$ in the 1.5 h prior to tornado touchdown. Following that, deeper layer 0–3 km helicity values abruptly increased to phenomenal values in excess of 750 $m^2 s^{-2}$ at the time of the tornado in response to both the strengthening of deep-layer vertical wind shear (and associated mid-tropospheric cooling seen by the radiometer) over the previous two hours and very rapid increases in low-level shear within 30 min of tornadogenesis.

Rapid destabilization worked in concert with the impressive increases in vertical wind shear and storm-relative helicity in the lowest 2 km of the troposphere to create conditions highly conducive to generation of strong tornadoes in a region and at a time when such events rarely occur. These results point to the tremendous value added by the temporal sampling unavailable with normal NWS rawinsonde releases, and the enhanced understanding that can be gained by having collocated thermodynamic and wind information available in such a manner.

6. Acknowledgements

The MP-3000A radiometer data is available from Radiometrics, Inc. at this website: http://radiometrics.com/data/uploads/2015/01/MP-12ch-auxTVsurface.csv. Raw and processed wind profiler and vLAPS data are available from the NOAA Global Systems Division of the Earth System Research Laboratory in Boulder, Colorado by anonymous ftp at: ftp aftp.fsl.noaa.gov (use your email address for the password) at the following directory: cd /divisions/fab/windsor_case. Interested parties can obtain assistance for data inquiries by contacting Hongli Jiang at hongli.jiang@noaa.gov. Most of the radiometer thermodynamic plots were produced using the RAOB software (www.raob.com). The authors wish to express their appreciation to Steve Albers and Yuanfu Xie of ESRL/GSD, who provided assistance with the WRF model setup and diagnostic analysis. Thanks are also due to John Shewchuk for assistance with the RAOB software and interpretations.

7. References

Albers, S., et al., 1996, The Local Analysis and Prediction System (LAPS): Analyses of clouds, precipitation, and temperature. *Wea. Forecasting, 11*, 273–287.

Atkins, N. , R. Wakimoto, C. Ziegler, 1998, Observations of the fine-scale structure of a dryline during VORTEX 95. *Mon. Wea. Rev., 126*, 525–550.

Benjamin, S. L., B. E. Schwartz, E. J. Szoke, and S. E. Koch, 2004, The value of wind profiler data in U.S. weather forecasting. *Bull. Amer. Meteor. Soc., 85*, 1871–1886.

Buban, M. S., C. L. Ziegler, E. R. Mansell, Y. P. Richardson, 2012, Simulation of dryline misovortex dynamics and cumulus formation. *Mon. Wea. Rev., 140*, 3525–3551.

________, C. L. Ziegler, E. N. Rasmussen, Y. P. Richardson, 2007, The Dryline on 22 May 2002 during IHOP: Ground-radar and in situ data analyses of the dryline and boundary layer evolution. *Mon. Wea. Rev., 135*, 2473–2505.

Chadwick, R. B., and N. Hassel, 1987, Profiler: The next generation surface-based atmospheric sounding system. Preprints, *Third Int. Conf on Interactive Information and Processing Systems for Meteorology*, New Orleans, LA, Amer. Meteor. Soc., 15–21.

Cimini, D., et al., 2006, Temperature and humidity profile retrievals from ground-based microwave radiometers during TUC. *Meteor. Zeitschrift, Vol. 15, No. 1*, 45–56.

________, et al., 2011, Thermodynamic atmospheric profiling during the 2010 Winter Olympics using ground-based microwave radiometry. *IEEE Trans. Geosci. Rem. Sens., 99*, 1–11.

________, et al., 2013, Mixing layer height retrievals by multichannel microwave radiometer observations. *Atmos. Meas. Tech., 6,* 2941–2951.

Dabberdt W. F., et al. 2005, Multifunctional mesoscale observing networks. *Bull. Amer. Meteor. Soc., 86,* 961–982.

Droegemeier, K. K., S. M. Lazarus, and R. Davies-Jones, 1993, The influence of helicity on numerically simulated convective storms. *Mon. Wea. Rev., 121*, 2005–2029.

Feltz, W. F., and J. R. Mecikalski, 2002, Monitoring high-temporal-resolution convective stability indices using the ground-based Atmospheric Emitted Radiance Interferometer (AERI) during the 3 May 1999 Oklahoma–Kansas tornado outbreak. *Wea. Forecasting, 17*, 445–455.

Geerts, B., et al., 2009, A case study of a long-lived tornadic mesocyclone in a low-CAPE complex-terrain environment. *Electronic J. Severe Storms Meteor., 4(3)*, 1–29.

Güldner, J., 2013, A model-based approach to adjust microwave observations for operational applications: results of a campaign at Munich airport in winter 2011/2012. *Atmos. Meas. Tech., 6,* 2879–2891.

________, and D. Spänkuch, 2001, Remote sensing of the thermodynamic state of the atmospheric boundary layer by ground-based microwave radiometry. *J. Atmos. Oceanic Technol., 18*, 925–933.

Hardesty, R. M., et al., 2012, Thermodynamic Profiling Technologies Workshop Report to the National Science Foundation and the National Weather Service. *NCAR Technical Note NCAR/TN-488+STR,* 80 pp.

Hartung, D. C., J. A. Otkin, R. A. Petersen, D. D. Turner, and W. F. Feltz, 2011, Assimilation of surface-based boundary layer profiler observations during a cool-season weather event using an Observing System Simulation Experiment. Part II: Forecast assessment. *Mon. Wea. Rev., 139,* 2327–2346.

Hewison, T., 2014, 1D-VAR retrieval of temperature and humidity profiles from a ground-based microwave radiometer. *IEEE Trans. Geosci. Rem. Sens., 45*, 2163–2168.

Hiemstra, et al., 2006, Comparing Local Analysis and Prediction System (LAPS) assimilations with independent observations. *Wea. Forecasting, 21*, 1024–1040.

Knupp, K. R. et al., 2009, Ground-based passive microwave profiling during dynamic weather conditions. *J. Atmos. Oceanic Technol., 26*, 1057–1073.

Koch, S. E., and J. McCarthy, 1982, The evolution of an Oklahoma dryline. Part II, Boundary layer forcing of mesoconvective systems. *J. Atmos. Sci., 39,* 237–257.

________, M. desJardins, and P. J. Kocin, 1983: An interactive Barnes objective map analysis scheme for use with satellite and conventional data. *J. Climate Appl. Meteor*., *22,* 1487–1503.

________, and W. L. Clark, 1999, A nonclassical cold front observed during COPS-91: Frontal structure and the process of severe storm initiation. *J. Atmos. Sci., 56*, 2862–2890.

Liljegren, J., S. Boukabara, K. Cady-Pereira and S. Clough, 2004, The effect of the half-width of the 22-GHz water vapor line on retrievals of temperature and water vapor profiles with a twelve-channel microwave radiometer. *IEEE Trans. Geosci. Rem. Sens.*, 1–7.

Madhulatha, A., et al. 2013, Nowcasting severe convective activity over southeast India using ground-based microwave radiometer observations. *J. Geophys. Res., 118*, 1–13.

McCarthy, J., and S. E. Koch, 1982, The evolution of an Oklahoma dryline. Part I, A mesoscale and subsynoptic-scale analysis. *J. Atmos. Sci., 39,* 225–236.

National Research Council, 2009, Observing Weather and Climate from the Ground Up: A Nationwide Network of Networks. Washington, DC: *The National Academies Press*.

________, 2010, When Weather Matters: Science and Service to Meet Critical Societal Needs. Washington, DC: *The National Academies Press*.

Otkin, J. A., D. C. Hartung, D. D. Turner, R. A. Petersen, W. F. Feltz, and E. Janzon, 2011, Assimilation of surface-based boundary layer profiler observations during a cool-season weather event using an Observing System Simulation Experiment. Part I: Analysis impact. *Mon. Wea. Rev., 139,* 2309–2326.

Rasmussen, E. N., and D. O. Blanchard, 1998, A baseline climatology of sounding-derived supercell and tornado forecast parameters. *Wea. Forecasting, 13*, 1148–1164.

Schumacher, R. S., et al., 2010, Multidisciplinary analysis of an unusual tornado: Meteorology, climatology, and the communication and interpretation of warnings. *Wea. Forecasting, 25,* 1412–1429.

Spänkuch, D., J. Güldner , H. Steinhagen and M. Bender, 2012, Analysis of a dryline-like feature in northern Germany detected by ground-based microwave profiling, *Met. Zeit*, *20 (4),* 409-421.

Szoke, E. J., et al., 1984, A subsynoptic analysis of the Denver tornadoes of 3 June 1981. *Mon. Wea. Rev., 112,* 790–808.

Thompson, R. L., et al., 2003, Close proximity soundings within supercell environments obtained from the Rapid Update Cycle. *Wea. Forecasting, 18*, 1243–1261.

Trexler, C. M., and S. E. Koch, 2000, The life cycle of a mesoscale gravity wave as observed by a network of Doppler wind profilers. *Mon. Wea. Rev., 128*, 2423–2446.

Wagner, T. J., W. F. Feltz, and S. A. Ackerman, 2008, The temporal evolution of convective indices in storm-producing environments. *Wea. Forecasting, 23*, 786–794.

Wakimoto, R. M., H. V. Murphey, E. V. Browell, and S. Ismail, 2006, The "triple point" on 24 May 2002 during IHOP. Part I: Airborne Doppler and LASE analyses of the frontal boundaries and convection initiation. *Mon Wea. Rev., 134*, 231–250.

Ware, R., et al., 2003, A multichannel radiometric profiler of temperature, humidity, and cloud liquid. *Radio Sci., 38*, *8079*.

________, 2013, Thermodynamic and liquid profiling during the 2010 Winter Olympics, *Atmospheric Research, Vol. 132–133*, 278–290.

Weckwerth, T. M., and D. B. Parsons, 2004, A review of convection initiation and motivation for IHOP_2002. *Mon. Wea. Rev., 134*, 6–22.

Weiss, C. C., and H. B. Bluestein, 2002, Airborne pseudo-dual-Doppler analysis of a dryline–outflow boundary intersection. *Mon. Wea. Rev., 130*, 1207–1226.

Wilson, J. W., N. A. Crook, C. K. Mueller, J. Sun, and M. Dixon, 1998, Nowcasting thunderstorms: A status report. *Bull. Amer. Meteor. Soc., 79*, 2079–2100.

Xie, Y. et al., 2011, A Space-Time Multiscale Analysis System: A sequential variational analysis approach. *Mon. Wea. Rev., 139*, 1224–1240.

Xu, G., et. al., 2014, Effect of off-zenith observations on reducing the impact of precipitation on ground-based microwave radiometer measurement accuracy, *Atmos. Res*. *140-141,* 85–94.

Ziegler, C. , W. Martin, R. Pielke, R. Walko, 1995, A modeling study of the dryline. J. *Atmos. Sci., 52,* 263–285.

________, et al., 2010: The impact of spatial variations of low-level stability on the life cycle of a simulated supercell storm. *Mon. Wea. Rev., 138,* 1738–1766**.**

8. Table 1

Data availability over 24 h from 21 – 22 May 2008

Data Sources	Availability (0 – 24 h)
Microwave Radiometer	0000 UTC – 2359 UTC
Wind Profiler	0000 UTC – 1600 UTC
vLAPS	1300 UTC – 2359 UTC

9. Figures

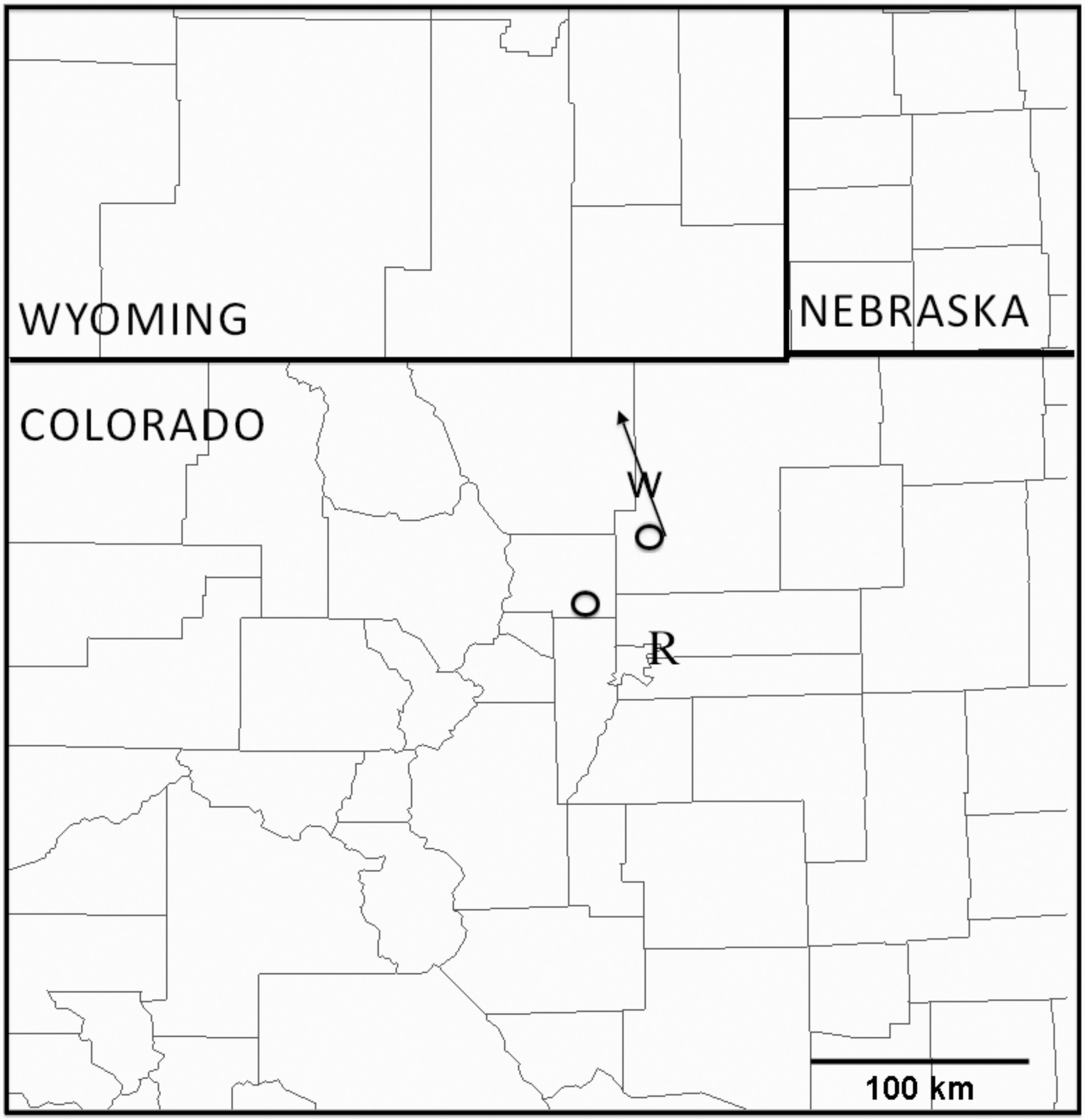

Figure 1. Map depicting domain of the vLAPS analyses, the locations of the microwave radiometer near Boulder, the wind profiler near Platteville, Colorado (the two small circles, with the profiler being the one farther northeast), the Denver NWS rawinsonde ("R"), and Windsor ("W"). The arrow indicates the general path of the Windsor tornado. The tornado touched down within 2 km of the wind profiler.

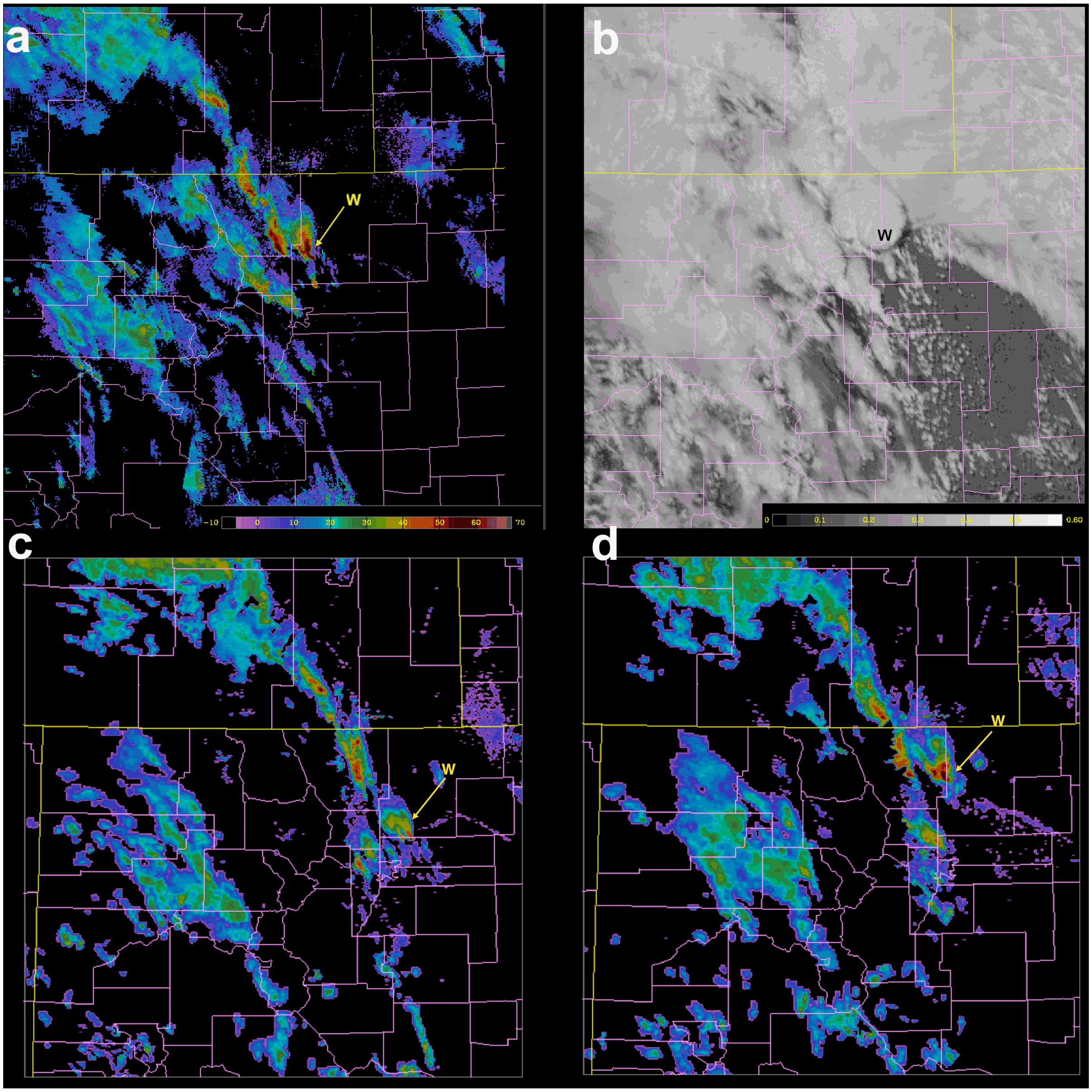

Figure 2. a) Radar reflectivity analysis from vLAPS multiple radar analysis and b) GOES visible albedo satellite imagery derived from vLAPS hydrometeor analysis at 1730 UTC 22 May 2008, c) vLAPS radar reflectivity analysis 30 min earlier (at 1700 UTC), and d) at 1800 UTC. The Windsor storm is shown with "W". Also noticeable to the west of Windsor are several other flow-parallel bands of deep convection (oriented northwest-southeast).

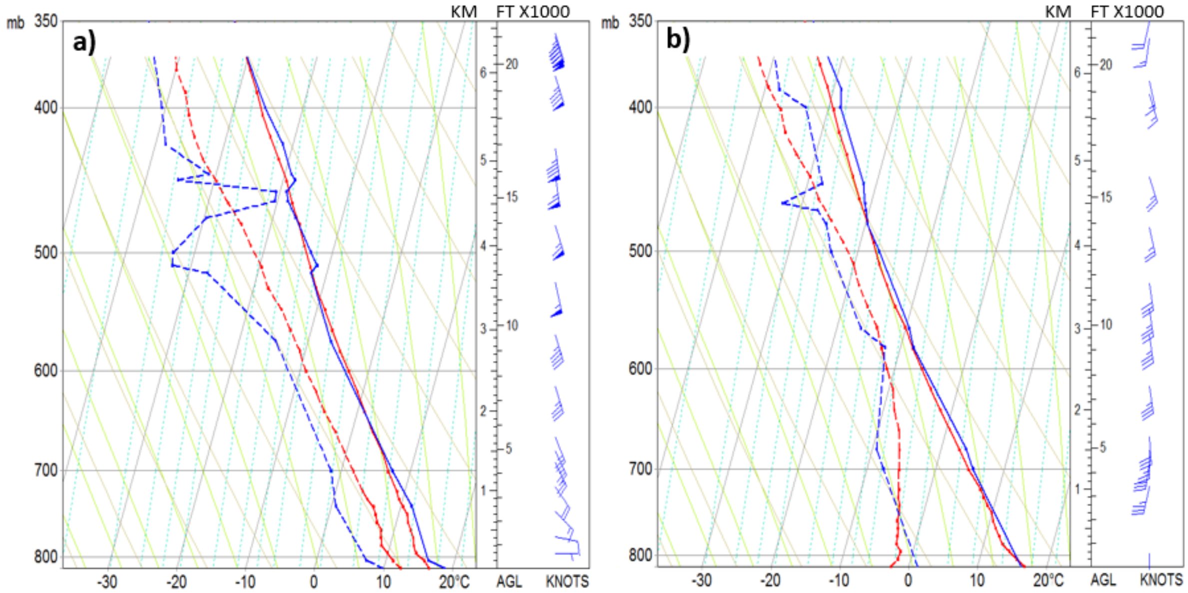

Figure 3. Skew-T plots of radiometer thermodynamic retrievals (red lines) and NWS-Denver (KDNR) soundings (blue lines) at a) 1800 UTC 22 May, and b) 0000 UTC 23 May from the 12-channel version of the radiometer. Displayed winds (kt) are from KDNR.

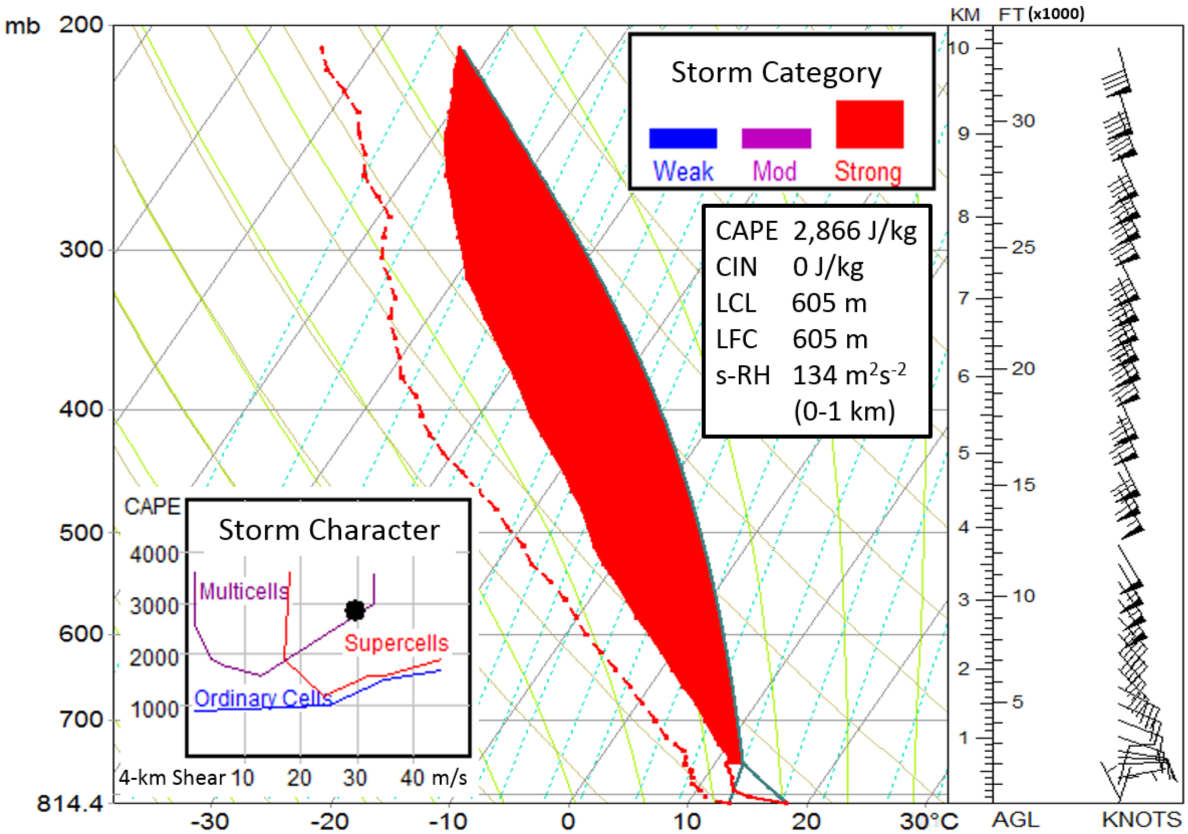

Figure 4. Sample radiometer sounding at 1706 UT showing lifted parcel positive area (red) to the right of the temperature profile. Computed Lifting Condensation Level (LCL) of 605 m matches the Level of Free Convection (LFC); thus there was no Convective Inhibition (CIN=0). Winds are taken from the 1800 UT Denver rawinsonde. Inset shows that the combination of 0–4 km wind shear (30 m s^{-1}) and Surface-Based CAPE (2866 J kg^{-1}) classifies this sounding as being indicative of supercell storm character. Storm-relative helicity is 134 (430) m^2 s^{-2} in the 0–1 km (0–3 km) layer. Plot was produced using the RAOB software analysis and display system (www.raob.com). RAOB "Storm Category" parameters indicate strong probability for severe convection.

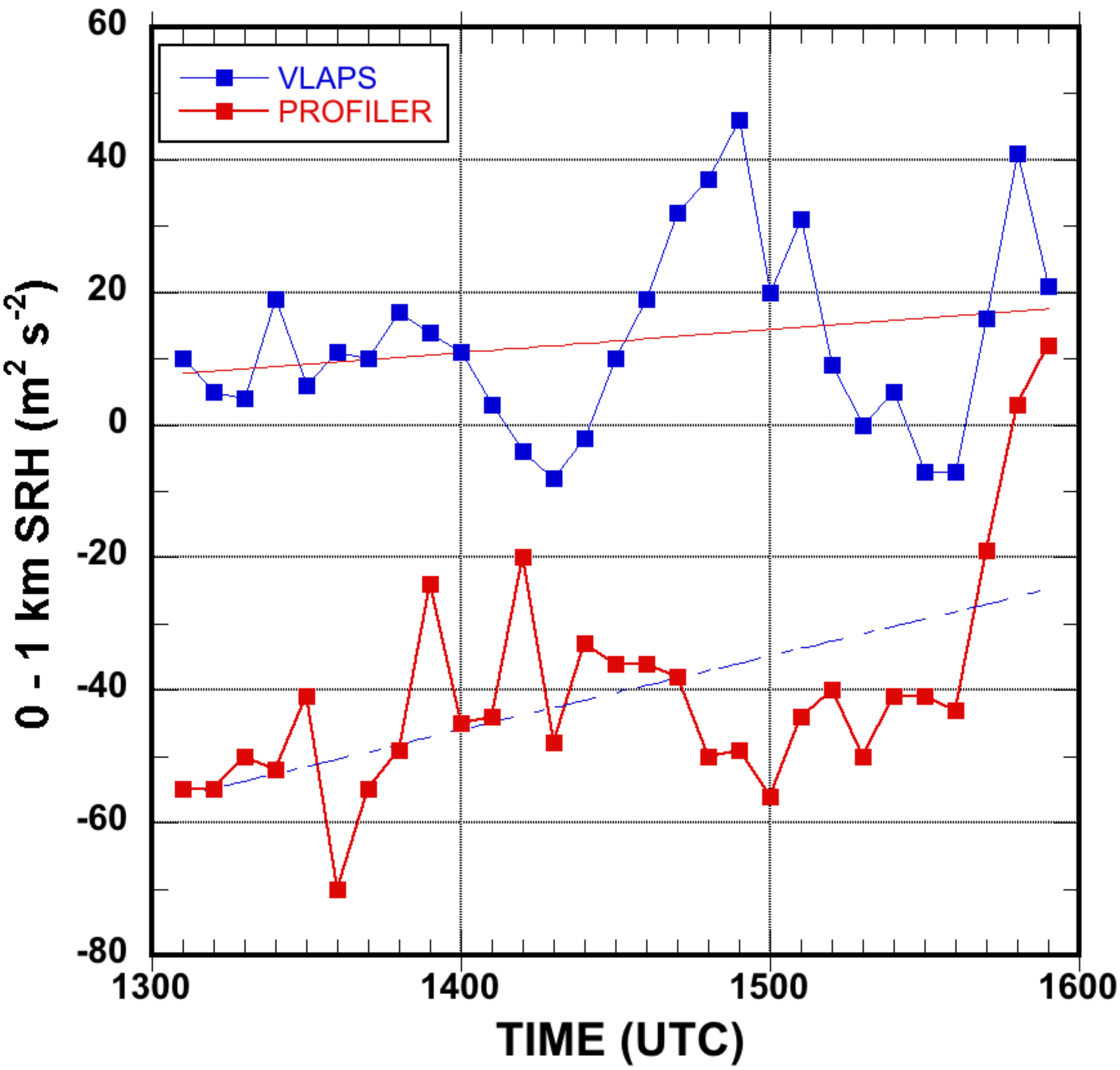

Figure 5. Comparison of time series of 0–1 km storm-relative helicity (SRH, m^2 s^{-2}) from Wind Profiler and vLAPS over the period 1310–1550 UTC. Linear lines of regression depict gradual upward trends in helicity values with time.

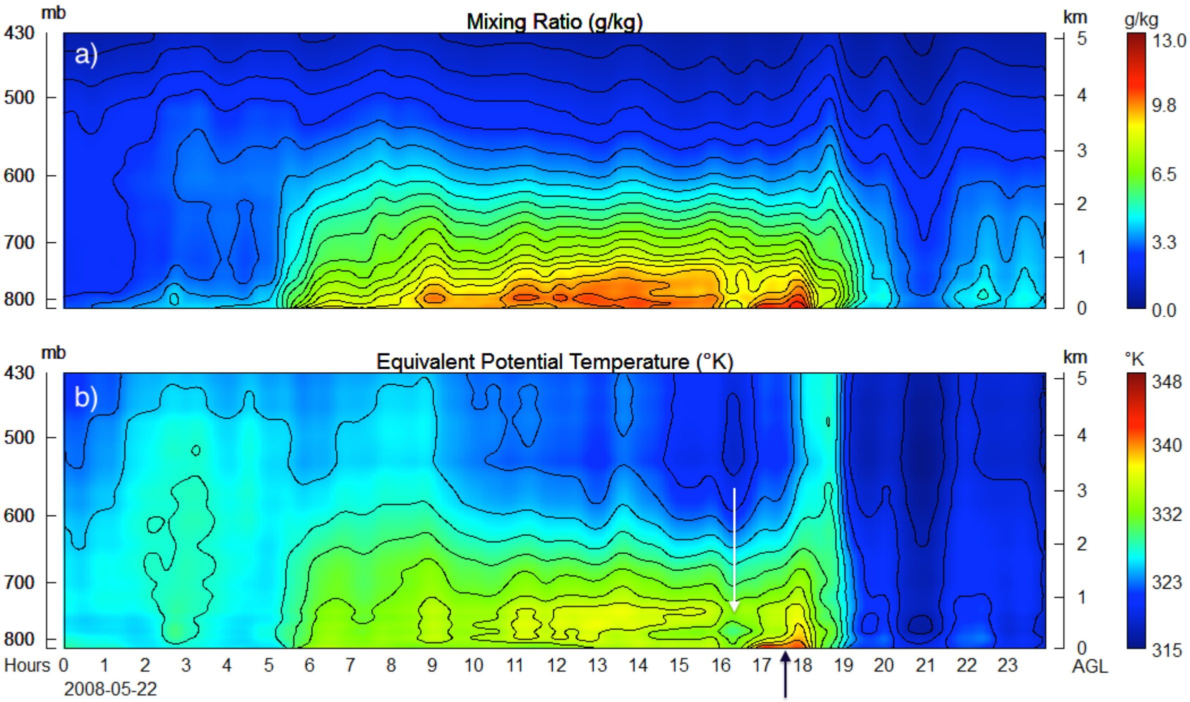

Figure 6. Time-height 24-h display beginning at 0000 UTC 22 May 2008 of a) water vapor mixing ratio (g kg^{-1}) and b) equivalent potential temperature (K) over the altitude range from the surface to 5 km AGL derived from the MP-3000 radiometer. Tornado touchdown occurs near the Platteville wind profiler site 30 km southeast of Windsor (47 km northeast of the radiometer) at approximately 1726 UTC, essentially at the time of occurrence of pronounced low-level moistening and destabilization. Dryline passes radiometer at 1840 UTC. White arrow denotes deep layer of destabilization resulting from mid-to-lower tropospheric decreases in equivalent potential temperature. Black arrow depicts rapid destabilization resulting from near-surface processes.

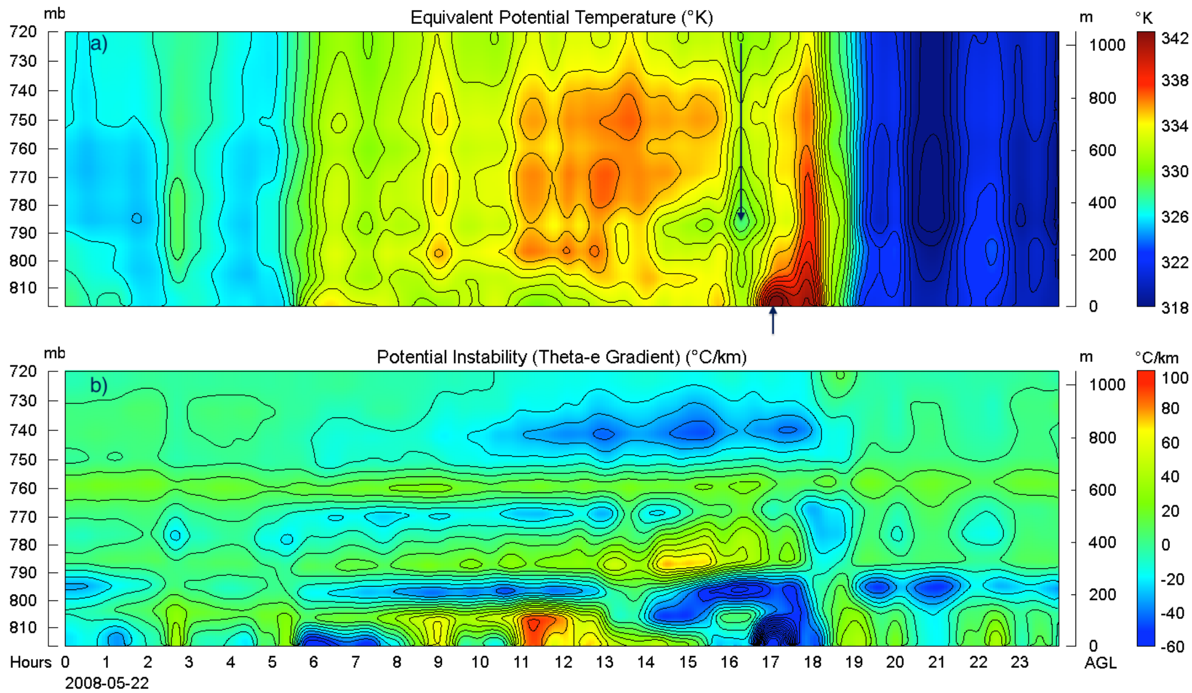

Figure 7. Variation over a 24 h period ending at 0000 UTC 23 May 2008 of potential instability (deg/km) calculated from the vertical gradient of equivalent potential temperature as derived from the radiometer over the 1000m layer immediately above the ground. Note the rapid destabilization in lowest 200 m after 1600 UTC with a strong maximum near the time of nearby tornado passage (1726 UTC). Black descending arrow denotes deep layer of destabilization resulting from mid-to-lower tropospheric decreases in equivalent potential temperature. Short black ascending arrow depicts rapid destabilization resulting from near-surface processes. Compare to equivalent potential temperature display in Fig. 6b.

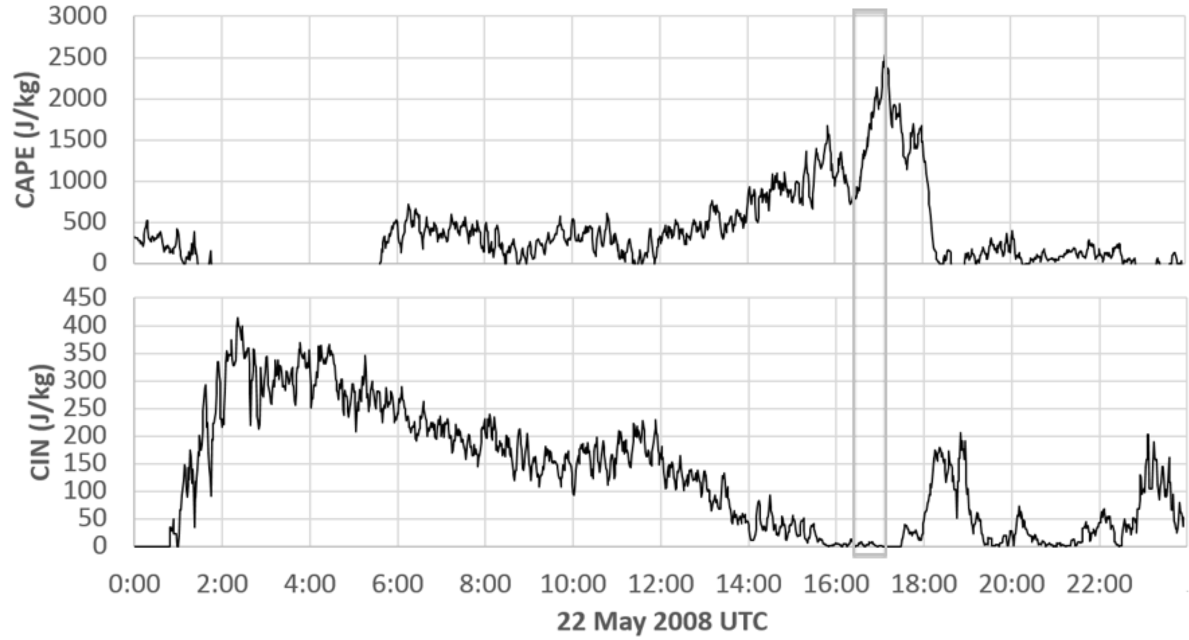

Figure 8. (top) 5-min filtered CAPE time series derived from radiometer showing gradual increase from 1200 to 1600 UTC, followed by a temporary decrease, a very pronounced increase just before tornado passage (1726 UTC), and a sudden decrease with passage of the dryline after 1800 UTC. The light gray box highlights the 45-min period during which the rapid increase in CAPE to its maximum value of 2550 J/kg occurred in conjunction with CIN = 0 (bottom). Actual peak value from unfiltered data was 2886 J/kg (Fig. 4).

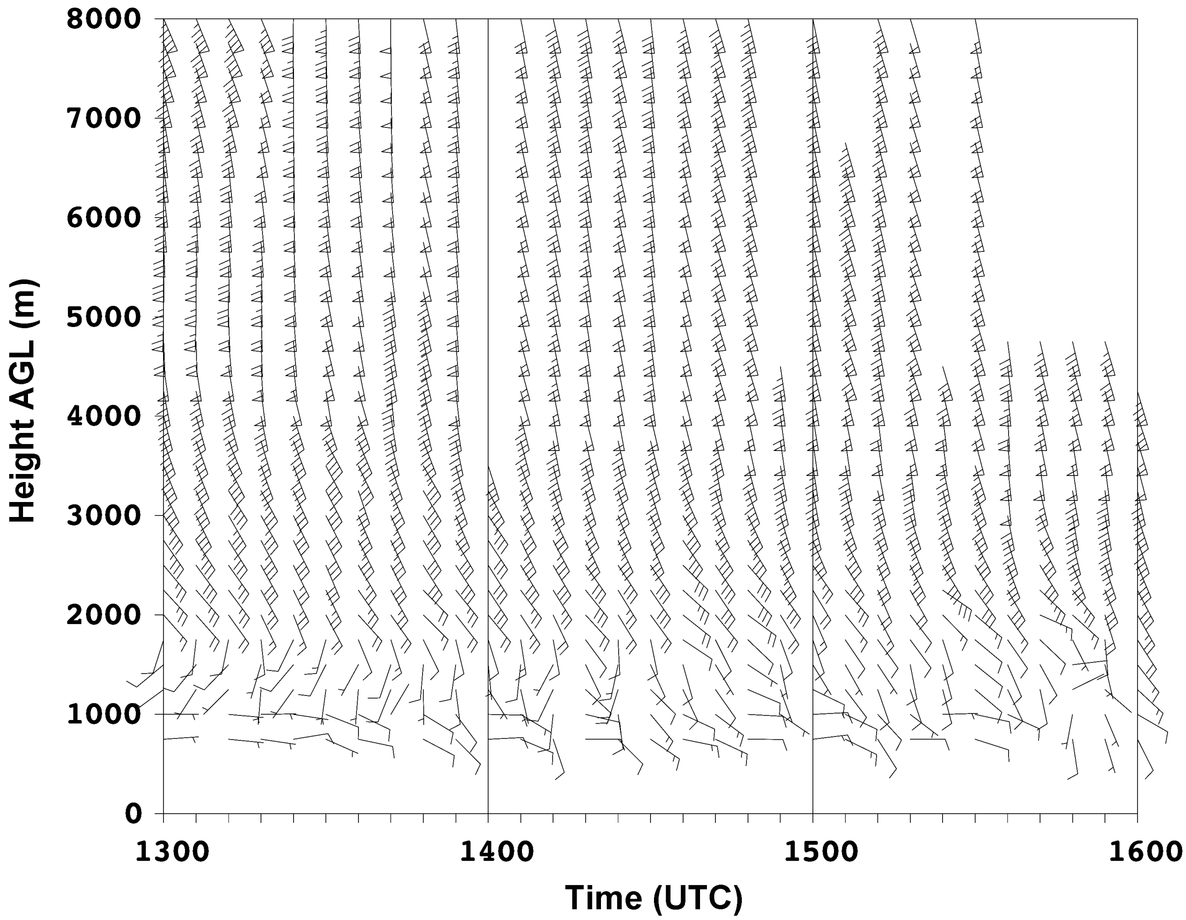

Figure 9. Time-height display of raw wind profiler data prior to quality control and objective analysis. Plot shows 6-min sampled horizontal wind vectors over the 0–8 km layer from 1300–1600 UTC, which is the last time data was available as the instrument was shut down in preparation for expected severe weather. Note this 3-h interval displayed is a subset of the 18h shown in Fig. 10a, and covers a different height range.

a)

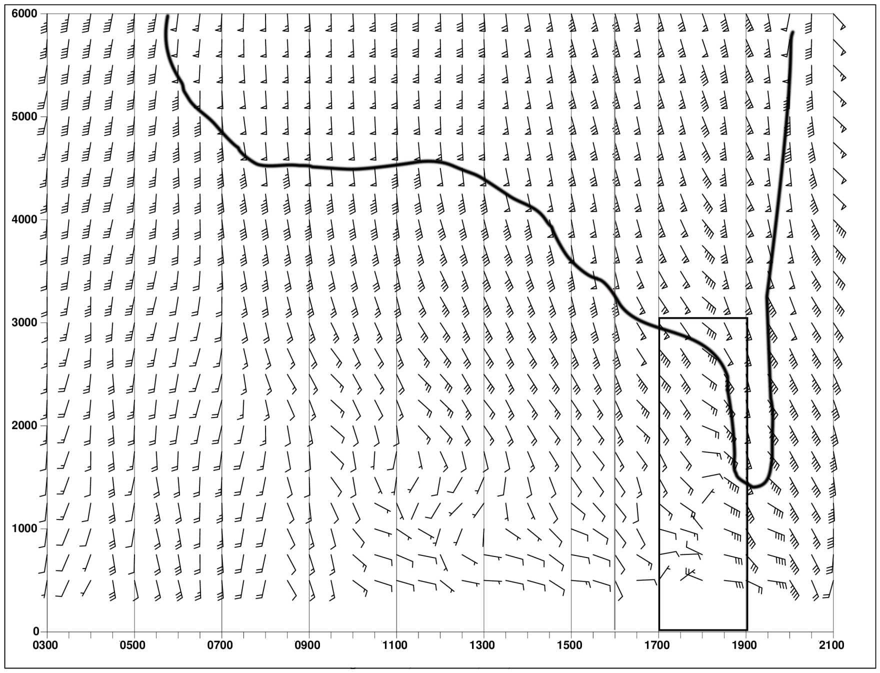

b)

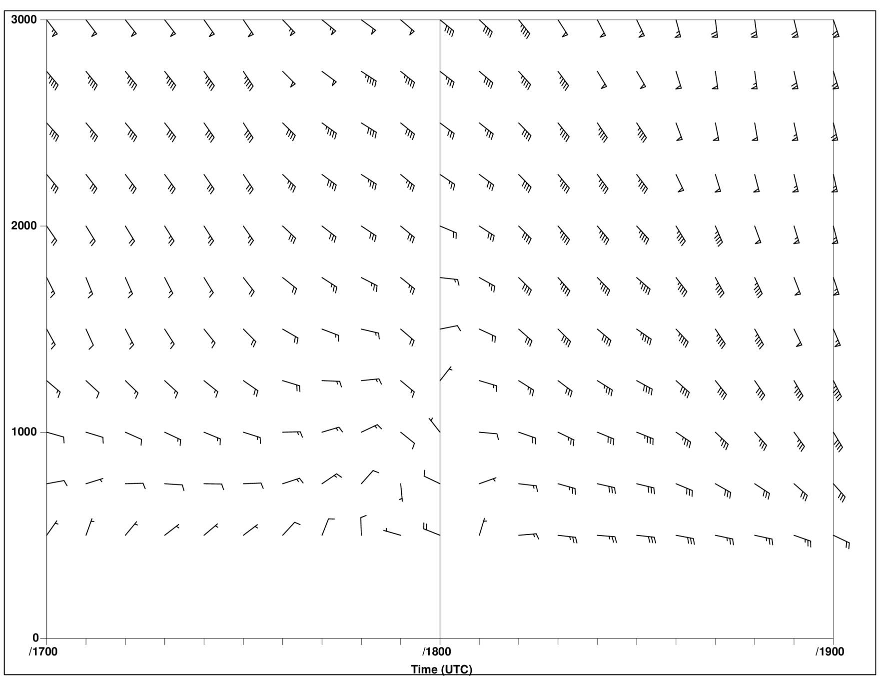

Figure 10. a) Merged time-height plot of horizontal winds following quality control and Barnes two-pass objective analysis of the wind profiler data, and merging of profiler winds before 1600 UTC with those from vLAPS afterwards through 2100 UTC (note light vertical line at the merger time). Data have been decimated to 30-min intervals. Curve represents subjectively analyzed 50-kt isotach; b) inset showing details within ±1h of 1800 UTC in the lowest 3 km of full 6-min resolution data.

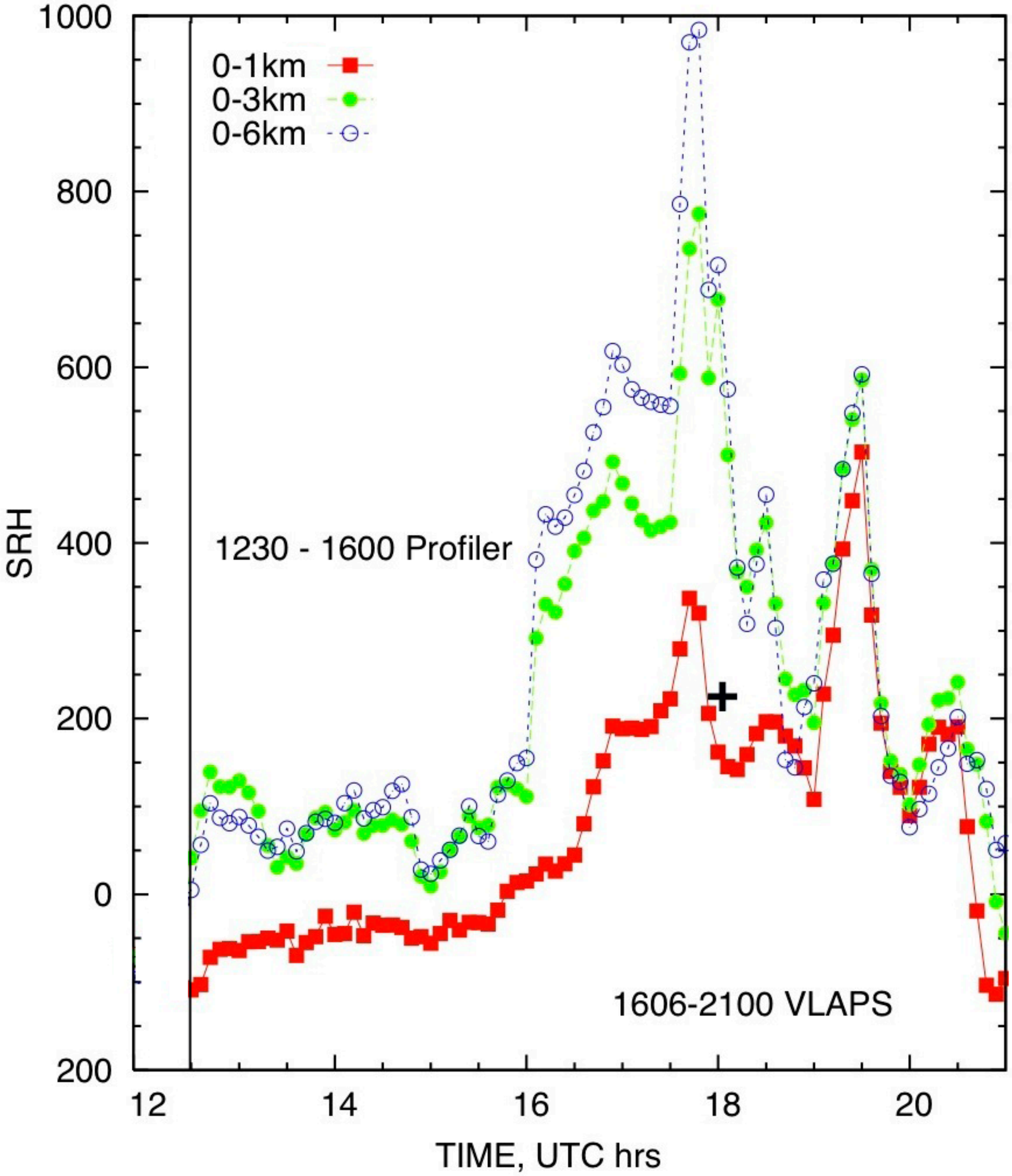

Figure 11. Time series of storm-relative helicity (SRH, $m^2\ s^{-2}$) for 0–1 km (red squares), 0–3 km (green circles), and 0–6 km layers (blue circles) computed from merged Wind Profiler and vLAPS datasets (Profiler from 1230–1600, vLAPS for 1606–2100 UTC). Black cross denotes 0–1 km helicity (219 $m^2\ s^{-2}$) estimated by *Schumacher et al.* [2010] upon modifying the 1800 UTC Denver sounding to account for the local conditions at Windsor.

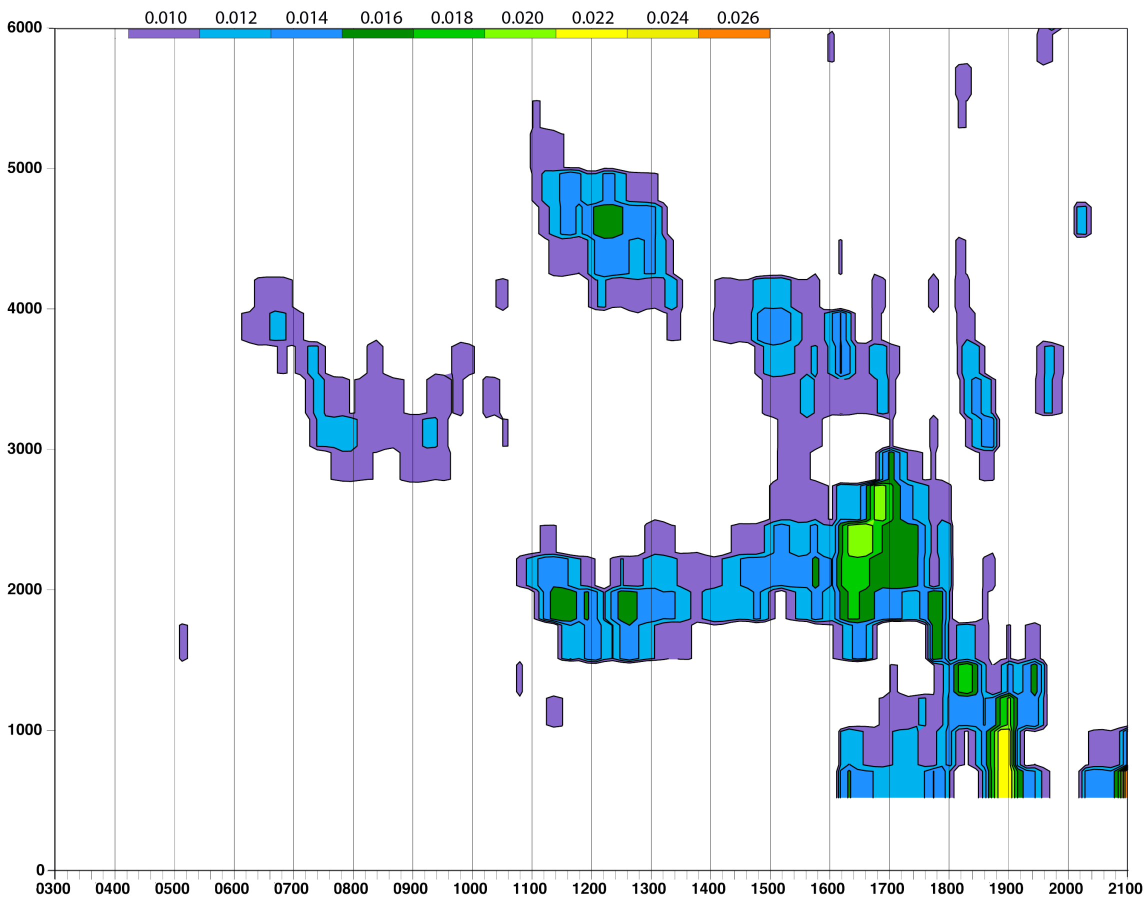

Figure 12. Time-height plot of vertical wind shear from merged profiler-vLAPS winds for the period 0300–2100 UTC at 12-min intervals. Note the descent of strong shear layer after 1300 UTC, rapid increase in shear in the 2.0–2.5 km layer after 1600 UTC, and sudden appearance of strong low-level shear at 1830 UTC associated with the appearance of strong winds from an east-southeasterly direction (cf. Fig. 10) immediately following the tornado. The extreme shear present as the tornado passed over the Profiler went undetected because of loss of Profiler data after 1600 UTC.